Vol. 599: 35–47, 2018
https://doi.org/10.3354/meps12614

MARINE ECOLOGY PROGRESS SERIES
Mar Ecol Prog Ser

Published July 12

Size-dependent phytoplankton growth and grazing in the northern South China Sea

Yuan Dong[1], Qian P. Li[1,2,*], Zijia Liu[1,2], Zhengchao Wu[1], Weiwen Zhou[1,2]

[1]State Key Laboratory of Tropical Oceanography, South China Sea Institute of Oceanology, Chinese Academy of Sciences, Guangzhou 510301, China

[2]University of Chinese Academy of Sciences, Beijing 100049, China

ABSTRACT: Field surveys of the northern South China Sea (NSCS) were conducted during the summer of 2015 and 2016 with size-fractionated chlorophyll *a* (chl *a*) measurements and size-specific dilution experiments for 3 phytoplankton size classes, including micro- (20 to 200 µm), nano- (2 to 20 µm), and picophytoplankton (<2 µm). Our results suggest that phytoplankton size structure and size-specific rates of growth and grazing mortality could vary substantially along the coastal, transition, and oceanic zones of the NSCS. There was an elevated microphytoplankton concentration in the inner shelf, in contrast to the dominance of nanophytoplankton over the middle and outer shelves. However, the phytoplankton community was mostly dominated by pico-cells in the oligotrophic oceanic regions. We found a nonlinear relationship between nanophytoplankton and total chl *a*, which is different from both pico-cells (a linear decrease) and micro-cells (a linear increase). By assessing the functional responses of the size-specific growth rates to nitrate concentrations, we found a higher nitrate-saturated maximal growth rate and a larger half-saturation constant for microphytoplankton, whereas nano- and picophytoplankton showed similar lower maximal rates and smaller half-saturation constants. There was also much higher grazing mortality of microphytoplankton in response to the increase in total chl *a*. These findings are important for understanding plankton dynamics and the associated biogeochemical fluxes in contrasting marine ecosystems, as well as for future size-structure modeling of the NSCS.

KEY WORDS: Size-fractionated chlorophyll · Size-specific phytoplankton growth · Microzooplankton grazing · South China Sea

INTRODUCTION

The size of plankton is crucial in many ecological processes, including regulating phytoplankton community compositions, determining energy flow of plankton food webs, and controlling biogeochemical cycles in the ocean (Ward et al. 2012). The size structure of the phytoplankton community also affects a variety of phytoplankton metabolic processes, such as growth, nutrient uptake, and respiration (Nielsen 2006, Marañón et al. 2007). In contrast to phytoplankton communities dominated by larger size classes in nutrient-replete coastal regions, primary production in oligotrophic regions is largely contributed by smaller-sized picoplankton (Chisholm 1992, Ciotti et al. 2002, Liu et al. 2007). This discrepancy may be due to the competitive advantage of large phytoplankton for growing in highly fluctuating nutrient environments (Malone 1980) and the advantage of small phytoplankton in acquiring sparse nutrients in low-nutrient environments (Sherr et al. 2005). Field investigations concerning size-specific phytoplankton growth in contrasting marine ecosystems are thus important for understanding the spatial and temporal variations of phytoplankton assemblages and associated biogeochemical transformations (Marañón 2015).

Microzooplankton grazing on average accounts for >60% of the phytoplankton loss in the ocean (Calbet

*Corresponding author: qianli@scsio.ac.cn

& Landry 2004). Grazing pressure from microzooplankton can vary with the change in phytoplankton size structure from nearshore to offshore (Landry et al. 2009). Microzooplankton (<200 µm) selective grazing on picophytoplankton (<2 µm), such as *Prochlorococcus* and *Synechococcus*, is common in eutrophic coastal waters (Strom et al. 2007). The preference of microzooplankton grazing, however, can switch from picophytoplankton to nanophytoplankton (2 to 20 µm), such as phytoeukaryotes, in oligotrophic waters and contribute to the dominance of picoplankton in the open seas (Cáceres et al. 2013, Zhou et al. 2015). Microzooplankton can also feed on microphytoplankton (20 to 200 µm) (Neuer & Cowles 1994, Sherr & Sherr 2009), although it is commonly grazed by mesozooplankton in the coastal ocean (Calbet & Saiz 2005). These grazing patterns can vary with different conditions, as microzooplankton grazing preference is also influenced by other factors such as phytoplankton growth rate, nutritient deficiency, and/or taxonomic affiliation (Strom 2002, Lie & Wong 2010, Cáceres et al. 2017).

The northern South China Sea (NSCS), one of the world's largest semi-enclosed seas, is influenced by a number of processes including seasonal monsoons, river discharge, coastal upwelling, atmospheric deposition, and Kuroshio intrusion (e.g. Jilan 2004), leading to a diverse nutrient environment over the shelf (Li et al. 2016). In addition to light and temperature, variations in nutrient availability driven by physical dynamics can affect growth rates of different phytoplankton size classes, as a result of the size-dependent nutrient acquisition of the phytoplankton community (Irwin et al. 2006, Marañón et al. 2007). It is the dynamic interaction between size-dependent growth and grazing that regulates the temporal change of size-fractionated phytoplankton biomass, and thus controls the size structure of phytoplankton community when processes such as sinking, advection, and aggregation are neglected (Taniguchi et al. 2014a). Substantial spatial and seasonal variations of phytoplankton size structure and taxonomy have been found in the NSCS by field measurements and by satellite remote sensing (Ning et al. 2005, Liu et al. 2007, Pan et al. 2013, Wang et al. 2015). However, mechanisms for the change in phytoplankton size structure in response to diverse environmental forcing remain largely unexplored in the NSCS.

In this study, the multi-treatment dilution technique (Landry & Hassett 1982) with modification of size-fractionated chlorophyll *a* (chl *a*) measurements (Taniguchi et al. 2012) were applied to study the surface phytoplankton community from coastal to oceanic regions of the NSCS during summer 2015 and 2016. Besides hydrographic and biogeochemical measurements such as temperature, salinity, nutrients, and chl *a*, the size structure of the phytoplankton community was also quantified by size-fractionated chl *a* measurements that separated the phytoplankton community into 3 major groups: picophytoplankton, nanophytoplankton, and microphytoplankton. Based on these field data, we addressed the spatial variability of phytoplankton community size structure and the associated size-dependent growth and grazing dynamics in the NSCS. It was our goal to explore the underlying factors controlling size-dependent plankton dynamics in the contrasting coastal and oceanic ecosystems, which is essential for understanding the trophic and biogeochemical functioning of the NSCS shelf sea.

MATERIALS AND METHODS

Description of the field study

Two field studies were conducted in the NSCS, one aboard R/V 'Shiyan III' in July 2015 and the other aboard R/V 'Zhanjiang Kediao' in June 2016. Phytoplankton size-fractionated chl *a* measurements of the water column were performed during the cruises from the surface to a depth of 150 m, along with comprehensive hydrographic and biogeochemical measurements from the inner shelf to the offshore region (sections A and B in Fig. 1). Temperature, salinity, and density data were obtained from a SeaBird SBE 9/11 CTD rosette sampling system, which collected seawater samples at the standard depths of 0, 25, 50, 75, 100, and 150 m for each station. Surface photosynthetically active radiation (PAR) was determined by a PAR sensor (400 to 700 nm irradiance, 2π) attached to the CTD. Size-fractioned multi-treatment dilution experiments were performed for the surface waters collected by Niskin bottles at 14 stations in the NSCS, covering the inner, middle, and outer regions of the continental shelf outside the Pearl River Estuary, as well as the offshore deep-basin regions with bottom depths >1000 m (Fig. 1, see Table 1).

Measurements of size-fractioned chl *a* and nutrients

The size-fractioned chl *a* of micro- (20 to 200 µm), nano- (2 to 20 µm) and picophytoplankton (<2 µm) were analyzed for waters at each depth. After removing large grazers (>200 µm) using a 200 µm mesh, du-

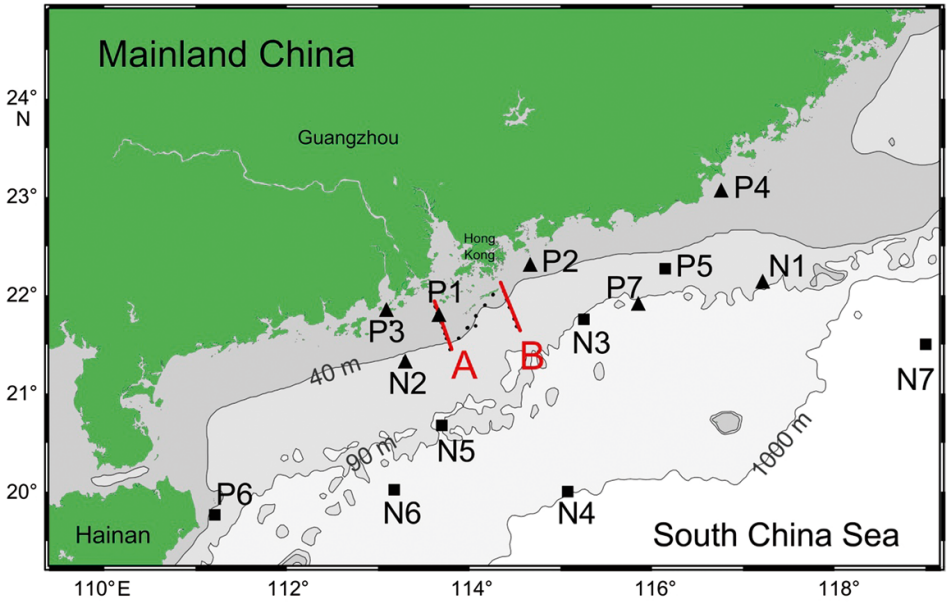

Fig. 1. Sampling map of the northern South China Sea. Squares and triangles: incubation stations for the summer of 2015 and 2016, respectively; 2 red lines show sections A and B, with small dots representing sampling stations; grey lines: 40, 90, and 1000 m isobaths; grey colors indicate bathymetry. P, N: surface chlorophyll concentration greater than or less than 0.5 µg l^{-1}, respectively

plicated seawater samples (1 to 2 l) were processed through a sequence of filtration steps under a low vacuum (<50 kPa), including a 20 µm pore size Nylon membrane filter, a 2 µm pore size polycarbonate filter, and a GF/F filter. Total chl *a* (Tchl *a*) was calculated as the sum of the chl *a* concentrations of the 3 different size classes. Particle-retained filters were extracted in 90% acetone for at least 18 h in the dark at –20°C. After centrifugation at 4000 rpm (1792 × *g*) for 10 min, the chl *a* concentration was determined by a Turner Designs Model 10 Fluorometer (Parsons et al. 1984). A 100 ml seawater sample for nutrients, including nitrate (NO_3^-), phosphate (PO_4^{3-}), and silicate (SiO_3^{2-}), was pre-filtered through GF/F filters, frozen immediately onboard and stored in a freezer at –20°C until analyzed in the laboratory after the cruises with a Seal AA3 autoanalyzer (Bran-Luebbe) using colorimetric methods (Hansen & Koroleff 1999).

Flow-cytometry analyses of picophytoplankton community

Aliquots of 2 ml *in situ* seawater samples from standard depths of the water column were fixed with 0.2% v/v buffered paraformaldehyde and frozen at –80°C in a liquid nitrogen container onboard until analyzed in the lab by flow cytometry (FCM) (Vaulot et al. 1989). Cell abundances of picoplankton, such as *Prochlorococcus* (PRO) and *Synechococcus* (SYN), were enumerated using a FACS Calibur cytometer (Becton-Dickinson), with different populations distinguished based on side-scattering (SS), and orange and red fluorescence (Olson et al. 1993). We used 1 µm diameter yellow-green fluorescent beads (Polysciences) as an internal standard; the flow rate was ~1 µl s^{-1} during the analyses based on a linear regression between elapsed time and the weight differences of the calibration tube. These data were used to investigate the variation of picophytoplankton community structure, to explain the spatial difference of the growth and grazing dynamics for picophytoplankton in the NSCS.

Size-specific multi-treatment dilution experiments

All the bottles, tubing, and carboys for the dilution experiment were soaked in 10% HCl for at least 24 h and rinsed with deionized water and *in situ* surface seawater before each experiment. At each of the selected stations, ~30 l of surface seawater was collected using an acid-washed polyethylene bucket; the contents of the bucket were gently drained through silicone tubing enclosed with a 200 µm Nitex screen (to remove meso- and macrozooplankton) into polycarbonate carboys. Particle-free water was prepared by gravity filtration of the above seawater through a 0.2 µm filter. The whole seawater was gently siphoned into 2.4 l polycarbonate bottles containing specific volumes of particle-free water to obtain a dilution series of 8, 37, 79, and 100% whole seawater. Each dilution treatment was duplicated during the experiment. Eight incubation bottles were enriched with dissolved inorganic nutrients of 0.5 µmol l^{-1} NH_4Cl, 0.03 µmol l^{-1} KH_2PO_4, 0.5 µmol l^{-1} Na_2SiO_3,

and 1 nmol l^{-1} $FeCl_3$ to ensure an adequate availability of these nutrients for phytoplankton growth. Two additional bottles of the whole seawater served as controls without nutrient addition. All these bottles were tightly capped and incubated for 24 h in a deck incubator with a neutral density screen to effectively reduce the impact of photoacclimation during the experiments (Zhou et al. 2015). The temperature was controlled by running surface seawater pumped from the sea surface. Aliquots of 1000 ml samples were taken from each bottle for chl *a* and nutrient measurements. The initial chl *a* concentrations of the diluted bottles were estimated from the whole seawater multiplied by the dilution factor.

Estimates of nutrient-amended phytoplankton growth rates (μ_n, d^{-1}) and microzooplankton grazing rates (g, d^{-1}) for each phytoplankton size class (Landry & Hassett 1982, Taniguchi et al. 2012) were calculated with least-square regression between the net growth rates (η, d^{-1}) and the dilution factors (D) as:

$$\eta_i = \frac{1}{t}\ln\left[\frac{Chl_i(t)}{Chl_i(0)}\right] = \mu_{n_i} - D \cdot m_i \quad (1)$$

where chl_i (0) and chl_i (t) represent the initial and final concentrations of chl *a* for the phytoplankton size-class i (1, 2, and 3 for micro-, nano-, and picophytoplankton, respectively); η_i, μ_{ni}, and m_i are the size-specific rates at the size-class i, and t is the incubation time, which is 24 h in our experiment. The natural phytoplankton growth rate (μ) was calculated as the sum of the net growth rate without nutrient enrichment (η_{raw}) and the grazing rate (m).

The data of the multi-treatment dilution experiments in the coastal and offshore regions of the NSCS were well fitted by the above linear regression model, as demonstrated by an r^2 of 0.7–1 (see Fig. S1 in the Supplement at www.int-res.com/articles/suppl/m599p035_supp.pdf). We did not include the growth and grazing rates of micro- and nano-cells in the oceanic zone and in some parts of the transition zone, as the initial chl *a* concentrations of micro- and nano-cells in these waters were close to the detection limit of our method (0.01 µg l^{-1}).

Size-fractionated maximal growth rate and half-saturation constant

Since the surface of the NSCS is generally nitrogen-limited (Chen et al. 2004), we focused on exploring the relationship between phytoplankton growth rate and nitrate concentration for all stations. We assumed the growth rate for each size class followed Michaelis-Menten kinetics, with a maximal growth rate μ_i^{max} and a half-saturation constant K_i (Li et al. 2010):

$$\mu_i = \mu_i^{max}\frac{[NO_3]}{K_i + [NO_3]} \quad (2)$$

where i represents the size class. Therefore, the growth rate will increase monotonically with nitrate concentration before reaching a saturation value of the maximal rate.

The best fit of Eq. (2) to the data (growth rate and nitrate) was accomplished in MATLAB (MathWorks) with 'fminsearch', which uses multidimensional unconstrained nonlinear optimization. The script finds the minimum of a cost function, starting at the initial estimate, and iterates the computations to return parameter values that minimize the cost function. We randomly assigned different initial guess values and found that the final optimal parameters (μ_i^{max} and K_i) were unchanged.

Statistical analysis

Data analysis was performed using the statistical software SPSS v.13.0 (SPSS) with figures constructed using Microsoft Excel 2003. A Student's *t*-test with a 2-tailed hypothesis was used when comparing 2 independent means. Pearson correlation analysis was applied to measure the strength and direction of the relationship between 2 environmental variables, and results were considered significant at $p < 0.05$. Comparisons between environmental variables were conducted using reduced major axis model II regression with r^2 representing the square of the Pearson coefficient of correlation. We assumed both regression variables were independent of each other. A permutation test was carried out to determine the significance of the slopes and to calculate the square of the Pearson correlation coefficients.

All the data used in the main article and Supplement, including water properties, growth and grazing rates, are available upon request (contact Q.P.L.).

RESULTS AND DISCUSSION

Spatial variations of water properties and phytoplankton size structure

Based on hydrographic and biogeochemical properties, surface waters in the NSCS can be roughly divided into 3 geographically distinct zones: the nearshore coastal zone, transition zone, and offshore

oceanic zone (Li et al. 2016). The coastal zone, characterized by high surface concentrations of nutrients and chl *a*, is subjected to the direct influences of both river outflow and coastal upwelling. The transition zone mostly encompasses the middle and outer shelves and can be affected by the Pearl River plume and its extension waters, whereas the offshore oceanic zone is close to the deep basin of the NSCS, with typical oligotrophic conditions in the upper euphotic zone. There was a relatively constant surface temperature of 29.7 ± 1.6°C (mean ± SD, hereafter) over the shelf during both summers. Surface PAR was also similar for the incubation stations, with a mean of 47.3 ± 2.0 E m^{-2} d^{-1} (Table 1), despite the broad sampling area. However, as a result of the river impact, surface salinity of 21.5 ± 10.7 in the coastal zone was much lower ($t = -2.67$, $p < 0.05$) than in the transition zone (31.3 ± 2.2) and oceanic zone (34.0 ± 0.1) (Table 1). We also found generally decreasing trends ($r^2 > 0.75$, $p < 0.05$) of surface nitrate and silicate concentrations with salinity from the coast to offshore, although the phosphate concentration was less variable (Table 1). The impact of the river plume was evident in the surface layer (<10 m), with strong salinity fronts over the edge between the coastal and transition zones (see Fig. S2a,d in the Supplement at www.int-res.com/articles/suppl/m599p035_supp.pdf).

There was considerable spatial variation of surface chl *a* during our studies in the NSCS (Fig. 2). Tchl*a* was the highest in the coastal zone with a mean of 3.63 ± 1.68 µg l^{-1}, followed by 0.59 ± 0.19 µg l^{-1} in the transition zone and 0.15 ± 0.05 µg l^{-1} in the oceanic zone. Size-fractionated chl *a* structure seemed quite variable, although there was a declining trend in the fraction of microphytoplankton ($r^2 = 0.35$, $p < 0.05$)

Table 1. Hydrographic and biogeochemical properties of the surface and bottom waters in the northern South China Sea (NSCS). Location of each station is shown in Fig. 1; sampling depth of surface water is always 1 m, but the depth of bottom water varies upon the local bathymetry. PAR: photosynthetically active radiation; Tchl*a*: total chlorophyll *a*; PRO: *Prochlorococcus*; SYN: *Synechococcus*; (—) no data

Stn	Depth (m)	*T* (°C)	S (psu)	PAR_0 (E m^2 d^{-1})	Tchl*a* (µg l^{-1})	NO_3 (µM)	PO_4 (µM)	SiO_4 (µM)	PRO (10^3 cells ml^{-1})	SYN (10^3 cells ml^{-1})
Coastal zone										
P1	1	29.5	21.0	45.9	4.36	9.4	0.12	9.3	—	—
	32	22.2	34.0	—	0.18	17.1	0.34	16.9	—	—
P2	1	29.4	23.5	47.4	4.43	5.3	0.12	4.9	—	—
	27	22.1	34.7	—	0.42	2.3	0.25	8.5	—	—
P3	1	31.8	7.8	46.2	4.60	44.4	0.07	69.7	—	—
	4	31.7	7.8	—	1.70	39.0	0.09	61.8	—	—
P4	1	26.2	33.7	50.5	1.11	10.0	0.08	10.3	—	—
	24	21.7	34.6	—	1.40	16.5	0.20	14.0	—	—
Transition zone										
P5	1	31.3	31.5	49.1	0.79	0.51	0.09	0.64	—	—
	44	21.1	34.5	—	0.40	5.80	0.40	7.20	—	—
P6	1	27.4	34.1	47.0	0.63	1.21	0.16	1.24	0.8	130.0
	40	18.8	34.6	—	0.42	13.5	0.69	10.1	67.8	0.9
P7	1	30.8	31.6	50.3	0.76	2.95	0.04	2.68	—	—
	85	20.1	34.7	—	0.00	4.73	0.28	7.05	—	—
N1	1	31.3	28.0	46.2	0.38	0.62	0.06	0.69	1.0	616.5
	74	19.1	34.8	—	0.05	3.08	0.36	3.28	—	—
N2	1	31.2	31.0	47.9	0.41	2.90	0.10	2.65	0.7	80.9
	38	21.7	34.6	—	0.83	2.15	0.17	6.32	—	—
Oceanic zone										
N3	1	29.9	33.9	47.8	0.24	0.37	0.01	1.55	661.4	109.5
	85	19.6	34.6	—	0.40	11.4	0.73	10.5	—	—
N4	1	29.4	33.9	46.0	0.12	0.60	0.08	1.95	111.9	65.7
	150[a]	16.1	34.6	—	0.03	15.5	0.81	11.5	6.4	1.1
N5	1	29.5	34.0	44.2	0.13	0.24	0.08	2.58	—	—
	75	20.4	34.6	—	0.49	9.06	0.48	8.67	—	—
N6	1	29.8	33.9	44.1	0.11	0.11	0.10	1.52	—	—
	119	17.6	34.6	—	0.10	7.92	0.52	7.44	—	—
N7	1	28.3	34.1	48.9	0.16	0.91	0.10	1.36	324.7	48.6
	150[a]	18.8	34.7	—	0.06	13.5	0.66	9.90	—	—

[a]These stations have bottom depths >1000 m (only data of 150 m are shown)

Table 2. Size-specific chl *a*, growth and grazing rates at the surface of the northern South China Sea (NSCS). nd: not detectable due to low chl *a*; dilution data for micro- and nano at Stn P3 were excluded due to lack of dilution factors <0.5; errors of the surface means are standard deviations; mean values and standard errors of μ_3 are calculated with negative rates excluded; location of each station is shown in Fig. 1; (—) no data

Stn	Micro (20 to 200 µm)				Nano (2 to 20 µm)				Pico (0.7 to 2 µm)			
	Chl_1%	μ_{n1}	m_1	μ_1	Chl_2%	μ_{n2}	m_2	μ_2	Chl_3%	μ_{n3}	m_3	μ_3
Coastal zone												
P1	63.8	2.9	3.8	2.4	24.5	2.4	2.9	1.6	11.7	2.1	2.3	1.7
P2	14.4	2.6	1.9	2.5	21.0	2.7	2.7	2.1	64.6	0.2	2.3	−0.2
P3	1.3	—	—	—	47.6	—	—	—	51.1	—	—	—
P4	34.2	4.5	3.4	2.9	28.8	3.7	3.1	2.5	37.8	3.0	2.5	1.7
Mean	28.4 ± 27.1	3.3 ± 1.0	3.0 ± 1.0	2.6 ± 0.3	30.5 ± 11.8	2.9 ± 0.7	2.9 ± 0.2	2.1 ± 0.5	41.3 ± 22.4	1.8 ± 1.4	2.4 ± 0.1	1.7 ± 0.1
Transition zone												
P5	16.5	0.4	0.7	0.4	43.9	1.1	0.9	0.9	39.2	1.3	1.0	1.1
P6	20.6	1.1	0.3	1.1	33.3	1.4	0.6	1.5	46.0	0.5	0.7	0.6
P7	2.6	nd	nd	nd	38.2	2.1	0.5	0.9	59.2	1.0	0.3	0.0
N1	7.9	nd	nd	nd	81.6	2.9	1.0	1.0	10.5	0.6	0.8	0.1
N2	4.9	nd	nd	nd	31.7	1.4	0.6	1.2	63.4	1.1	0.8	0.7
Mean	10.5 ± 7.8	0.8 ± 0.5	0.5 ± 0.3	0.7 ± 0.5	45.8 ± 20.5	1.8 ± 0.7	0.7 ± 0.2	1.1 ± 0.2	43.7 ± 20.9	0.9 ± 0.3	0.7 ± 0.3	0.6 ± 0.4
Oceanic zone												
N3	2.8	nd	nd	nd	12.5	nd	nd	nd	85.3	0.4	0.2	1.2
N4	5.7	nd	nd	nd	11.4	nd	nd	nd	82.9	0.4	0.1	0.2
N5	3.7	nd	nd	nd	10.0	nd	nd	nd	86.4	0.6	0.2	0.4
N6	4.3	nd	nd	nd	12.0	nd	nd	nd	81.8	0.3	0.2	0.2
N7	3.1	nd	nd	nd	15.3	nd	nd	nd	84.0	0.7	0.6	0.7
Mean	3.9 ± 1.1	—	—	—	12.1 ± 1.9	—	—	—	83.9 ± 1.9	0.5 ± 0.2	0.2 ± 0.2	0.5 ± 0.4

and an increasing trend in the fraction of picophytoplankton (r^2 = 0.38, $p < 0.05$) with salinity from the coast to offshore when Stn P3 was excluded (very low salinity) (Table 2, Fig. 2). On average, picophytoplankton could make up 84% of the Tchl *a* in the oceanic zone during the summer, which was consistent with that of ~80% found at the central NSCS (Liu et al. 2007). The cross-shelf variation of community size-structure could be more clearly seen from 2 additional 2-dimensional (2D) sections, with higher resolution sampling from the inner shelf to the outer shelf (see Fig. S2 in the Supplement). There were high concentrations of TChl *a* and high percentages of microphytoplankton in the coastal zone (Fig. S2b,e) associated with the low salinity river plume (Fig. S2a,d). At ~20 m depth in the water column, we also found subsurface intrusion of the oceanic community, with a high percentage of picophytoplankton but low percentages of micro- and nanophytoplankton while crossing the shelf toward the coast (Fig. S2c,f). There were large increases in the picophytoplankton proportion from 11 to 76% at section A and 27 to 78% at section B, respectively. The increased fraction of picophytoplankton was accompanied by a decreased fraction of microphytoplankton during both transects.

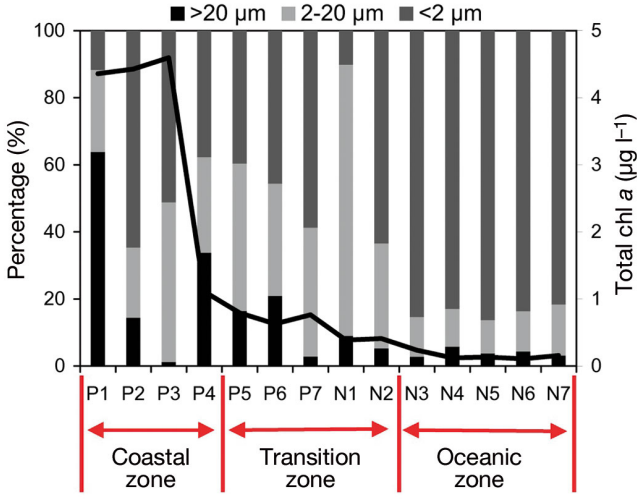

Fig. 2. Total chl *a* and size-fractionated percentage of the surface phytoplankton of the northern South China Sea during summer 2015 and 2016. Black line: chl *a* concentration; columns indicate percentages. Data are grouped into coastal, transition, and oceanic zones based on Fig. 1

Prior work reported that the dominant phytoplankton group shifted from diatoms in the inner shelf to small phytoplankton such as *Prochlorococcus* and *Synechococcus* in the open NSCS (Pan et al. 2013). Although picophytoplankton was the dominant class in the oceanic regions of the NSCS, its community structure varied substantially in the surface waters during our surveys. Offshore stations over the transi-

tional zone (such as Stns P6, N1, and N2) had high surface *Synechococcus* abundance, but negligible *Prochlorococcus*, whereas low *Synechococcus* and high *Prochlorococcus* were found in the surface waters at oceanic Stns N3, N4, and N7 (Table 1). For the vertical pattern of picophytoplankton, previous studies have found that *Synechococcus* may concentrate in the surface layers, while *Prochlorococcus* concentrates at the bottom of the euphotic zone in the open NSCS (Chen et al. 2009). At Stns P6 and N4, we indeed found an increase in *Prochlorococcus* at the base of the euphotic zone but a general decrease in *Synechococcus* with depth within the euphotic zone (Fig. S3).

Size-specific phytoplankton growth and microzooplankton grazing rates

There were large spatial variabilities in the size-specific growth and grazing rates in the NSCS (Table 2). Growth rates of microphytoplankton and nanophytoplankton in the nearshore coastal zone were 2.6 ± 0.3 and 2.1 ± 0.5 d^{-1}, respectively, which were much higher ($t > 3.97$, $p < 0.05$) than their rates of 0.7 ± 0.5 and 1.1 ± 0.2 d^{-1} in the transition zone, likely reflecting the high nutrient input nearshore by river plume and coastal upwelling (Huang et al. 2011). There was also an increase in the growth rate of picophytoplankton ($t = 3.06$, $p < 0.05$) from the transition and oceanic zones to the coastal zone of the NSCS. We did not find significant differences in picoplankton growth rates ($p = 0.44$, 1-tailed *t*-test) between the transition zone (*Synechococcus* comprised >90% of abundance) and the oceanic zone (*Prochlorococcus* comprised >65% of abundance), although it has been previously suggested that *Synechococcus* might grow much faster than *Prochlorococcus* in the NSCS (Chen et al. 2009).

In agreement with the growth rates, microzooplankton grazing on the 3 size classes all showed higher rates in the coastal zone and lower rates in the transition and oceanic zones, probably due to the tight prey–predator interaction (Chen et al. 2009). In general, there was a positive correlation between growth and grazing rates in the NSCS ($r^2 = 0.46$, $p < 0.05$) (Fig. S4), which should reflect the important role of microzooplankton grazing on primary production lost in the ocean (Calbet & Landry 2004). Large residuals around the regression line could be caused by processes that would lead to uncoupling between growth and grazing rates, such as chemical, morphological, and nutrient deficit defenses of phytoplankton to microzooplankton grazing (Strom 2002, Strom et al. 2007). The average high coupling of ~80% (the slope of the regression) during our study was consistent with previous results (e.g. Huang et al. 2011). The remaining ~20% of daily primary production could be consumed by mesozooplankton grazing (Chen et al. 2015) or lost by other processes such as sinking and advection.

Size-selective grazing by microzooplankton is important for shaping phytoplankton community structure, and thus regulates the primary production of the ocean (Kuipers & Witte 1999). In the coastal NSCS, we did not find the general decrease in microzooplankton grazing impact (m/μ ratio) with phytoplankton cell size suggested by Chen & Liu (2010). The average grazing impact for picophytoplankton was 1.4 ± 0.1 in the coastal zone with the negative values excluded. This value was not significantly different ($p > 0.25$, 1-tailed *t*-test) from that of nanophytoplankton (1.4 ± 0.5) and microphytoplankton (1.1 ± 0.4), although it had been previously suggested that microzooplankton might prefer to graze on small cells such as picophytoplankton in the eutrophic coastal ocean (Strom et al. 2007). Interestingly, we found a clear decrease ($t < -2.28$, $p < 0.05$) of grazing impact for picophytoplankton, from 1.4 ± 0.1 in the coastal zone to 1.0 ± 0.1 in the transition zone, and to 0.6 ± 0.3 in the oceanic zone. The reduced grazing pressure on smaller cells from coastal to oceanic zones is consistent with the observed shift of phytoplankton size structures, from large phytoplankton-dominated nearshore to picoplankton-dominated offshore, which is also in agreement with previous reports in the subtropical Northeast Atlantic (Cáceres et al. 2013). A low grazing impact of microzooplankton on picophytoplankton in the oceanic zone would result in its slow turnover rate, thus favorable for biomass buildup of small cells in the open seas (Zhou et al. 2015). In contrast, the enhanced grazing impact of pico-cells in the coastal zone should support the dominance of larger cells there (Strom et al. 2007).

Relationship between phytoplankton size structure and Tchl *a*

An understanding of the factors regulating size structure of the phytoplankton community has long been of interest to oceanographers (e.g. Thingstad 1998). Existing knowledge suggests that phytoplankton size structure could vary as a function of the concentration of Tchl *a*, which was believed to reflect a

community response to the change of total nutrients in the planktonic ecosystem (Chisholm 1992, Thingstad 1998, Goericke 2011a). Ideally, when the upper limit of a certain phytoplankton size class is reached, biomass can be further added to the next largest size class until its biomass upper limit is reached as well (Thingstad 1998), which will result in dominance of the smallest cells at low biomass.

Indeed, when Tchl *a* is low, small-sized picophytoplankton dominate the phytoplankton community in many parts of the ocean (e.g. Chisholm 1992). There is also evidence suggesting that with an increase in Tchl *a*, the fraction of picophytoplankton decreases substantially along with a large increase of microphytoplankton (Brewin et al. 2010, Goericke 2011b). In agreement with many of these field results (Chisholm 1992, Brewin et al. 2010, Goericke 2011b), we found a lower percentage ($r^2 = 0.13$, $p < 0.05$) of picophytoplankton Tchl *a* when the Tchl *a* was >1.0 µg l^{-1}, which was mirrored by a higher percentage ($r^2 = 0.31$, $p < 0.05$) of microphytoplankton (Fig. 3A,B). The threshold value of 1.0 µg l^{-1} we found for picophytoplankton in the NSCS was in agreement with previous findings (Raimbault et al. 1988, Goericke 2011b).

The response of the intermediate size class (nanophytoplankton) to increasing Tchl *a* is still debated. There are some studies indicating a linear increase of the nanophytoplankton fraction with respect to Tchl *a* (e.g. Goericke 2011b), while others have found a sinusoidal relationship between the nanophytoplankton fraction and Tchl *a* with the presence of a discrete biomass threshold (Raimbault et al. 1988, Brewin et al. 2010). Accurate determination of the relationship between the nanophytoplankton fraction and Tchl *a* could be essential for modelling the spatial and temporal change of phytoplankton size structure from remote sensing observations (Brewin et al. 2010). However, neither the linear relationship (Goericke 2011b) nor the sinusoidal relationship (Thingstad 1998, Brewin et al. 2010) for nanophytoplankton is supported by our data. In fact, the plot of the nanophytoplankton fraction versus Tchl *a* was rather scattered and showed the combined features of both picophytoplankton and microphytoplankton (Fig. 3A,B). In particular, there were some high percentages of nanophytoplankton found when Tchl *a* was <1.0 µg l^{-1}.

The major nanophytoplankton occupying the NSCS shelf are *Cryptophytes* and *Haptophytes* (mainly *Prymnesiophytes*), as revealed by pigment taxonomy (Wang et al. 2015). While *Cryptophytes* increases linearly with Tchl *a* just like with diatoms, *Prymnesiophytes* generally decreases with Tchl *a* when Tchl *a* is >1 µg l^{-1} (Goericke 2011a), similar to what we found for picophytoplankton. We thus expect to have 2 sub-groups within the nano-cell, one resembling microphytoplankton and the other, picophytoplankton, in response to increasing Tchl *a*. Indeed, the intermediate size class of 2–20 µm could be divided into 2 additional groups of 2–5 and 5–20 µm with very different slopes when plotted against Tchl *a* (Ciotti et al. 2002). Therefore, our results of nanophytoplankton from size-fractionated chl *a* measurements are in agreement with the pigment taxonomy of the NSCS. These results also imply that pigment

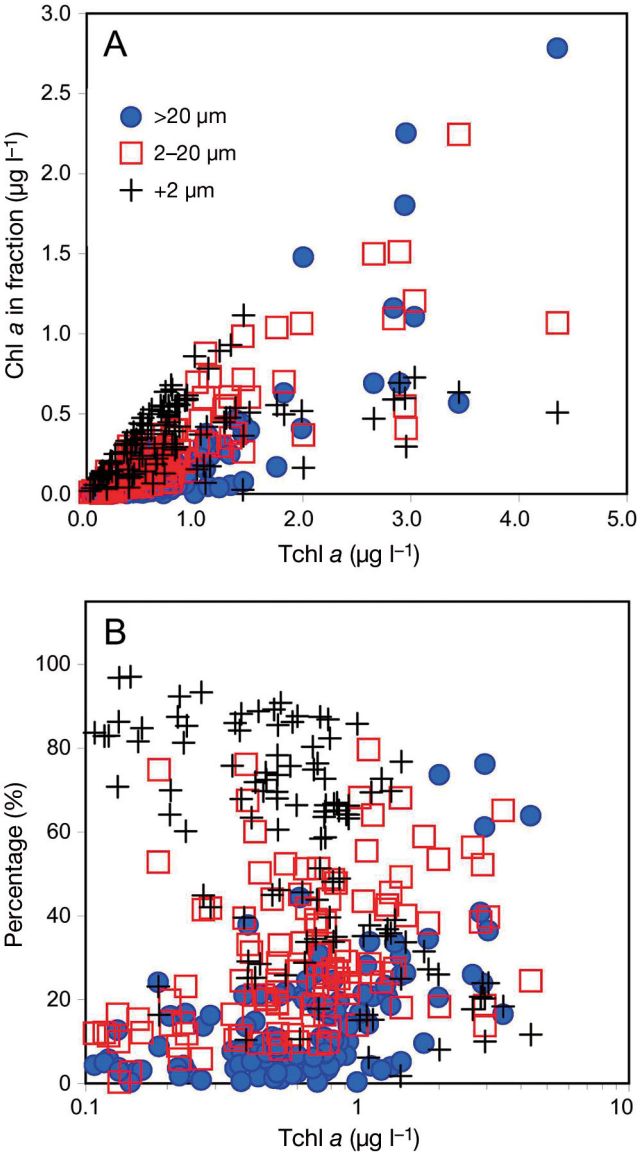

Fig. 3. Relationships of the (A) size-fractionated chl *a* and (B) corresponding percentage with total chl *a* in the northern South China Sea

taxonomy should be considered for accurately predicting phytoplankton size-structure from sea surface chl *a* concentration.

Responses of size-specific phytoplankton growth to varying nutrient concentrations

The growth rate of phytoplankton is controlled by factors such as temperature, light, nutrients, and community structure (Li et al. 2010). The environmental setup of the surface NSCS, with relatively constant surface PAR and temperature during our study periods, provides an opportunity to assess the functional response of the size-fractioned growth rate to the ambient nutrient concentration in the NSCS. There was a shift in the phytoplankton community from phosphorus stress off the coast to nitrogen stress offshore, as indicated by the surface N:P ratio (Table 1). In the coastal region, the most deficient nutrient will not become limiting as long as it remains replete (Moore et al. 2013). Since nitrogen is the most limiting nutrient over the large area of the NSCS shelf (Wu et al. 2003, Chen et al. 2004), we thus focused on exploring the relationship between growth rate and nitrate. We did not include ammonium in our analyses since the ammonium concentration tend to be much lower than nitrate in the surface NSCS (e.g. Wu et al. 2003). We fitted the data of growth rates and nitrate concentrations to the nonlinear Eq. (2) for each phytoplankton size class. All 3 size classes could be well fitted by the model ($p < 0.05$), with r^2 values of 0.51, 0.46, and 0.96 for pico-, nano-, and microphytoplankton, respectively (Fig. 4A–C). Based on the nonlinear fitting exercises, we also estimated the values of μ_i^{max} and K_i for each size class, as well as their uncertainties.

There was an increase ($t > 1.8$, $p < 0.05$) of phytoplankton maximal growth rate with cell size, from 1.9 ± 0.2 d^{-1} for pico-, to 2.1 ± 0.2 d^{-1} for nano-, and to 3.5 ± 0.3 d^{-1} for microphytoplankton in the NSCS. These values are comparable to their nutrient-amended growth rates of μ_n in the coastal zone (Table 2), given that the high level of nutrients there would lead to their nutrient-saturated growths. Our results support the increase of maximal specific photosynthetic rate for large phytoplankton under high nutrient, sufficient light, and constant temperature conditions (Cermeño et al. 2005). The deviation from the general allometric scaling theory (large sizes correspond to lower rates) with an increase in growth rate with cell size had been attributed to taxonomic

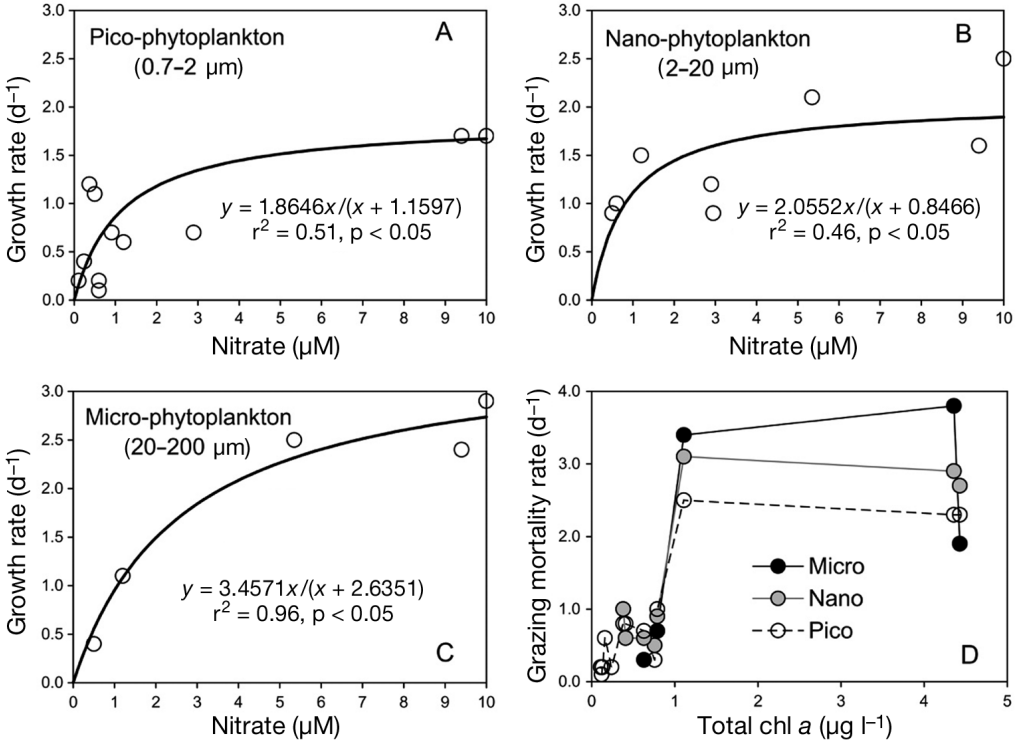

Fig. 4. Responses of the size-specific growth rates, including (A) pico-, (B) nano-, and (C) microphytoplankton, to varying nitrate concentrations; and (D) dependences of the size-specific grazing mortality rates on total chl *a*. Maximal rates and half-saturation constants are also reported; see 'Materials and methods: Size-fractioned maximal growth rate and half-saturation constant' for details

changes in the phytoplankton community along the size spectrum (Marañón et al. 2007, Chen & Liu 2010). Large phytoplankton such as diatoms could override the constraints of cell size with several strategies, including chain formation, changing cell shape, forming a vacuole, and increasing nutrient storage capacity (Stolte et al. 1994, Pahlow et al. 1997, Thingstad et al. 2005, Verdy et al. 2009). The half-saturation constant of 2.6 ± 0.6 µM for microphytoplankton in the NSCS is much higher ($t > 5.1$, $p < 0.05$) than 0.8 ± 0.2 µM for nanophytoplankton, and 1.2 ± 0.4 µM for picophytoplankton, which is also in agreement with a previous finding of an increase of the half-saturation constant with cell size for phytoplankton nutrient uptake (Litchman et al. 2007).

In the coastal zone, large phytoplankton (high μ^{max}) would grow faster than small phytoplankton (lower μ^{max}) when nutrients are replete. This would be an advantage for microphytoplankton to compete against other phytoplankton since the grazing impact was not significantly different among various size classes in the coastal zone. Hence, microphytoplankton can dominate the phytoplankton community in the eutrophic coastal waters of the NSCS. However, large phytoplankton with a greater K would be at a disadvantage in the transition and oceanic zones due to a stronger nutrient limitation. Small phytoplankton, such as nano- and picophytoplankton, can more easily survive in these waters, as their low K would allow them to attain a low resource requirement in the nutrient-deficient environments. Therefore, the lower K of small phytoplankton is responsible for their dominance in the offshore NSCS. For picoplankton, their success in the oceanic zone was also attributed to a reduced grazing impact compared to that of the coastal zone. Thus, picoplankton growth could still balance their grazing loss in the oceanic waters leading to tight coupling between growth and grazing. These findings support the previous argument that the most universally successful strategy of phytoplankton is one that can simultaneously optimize nutrient uptake and predator defense in the pelagic marine food web (Thingstad et al. 2005).

Our size-specific maximal growth rates of picophytoplankton are higher than those reported in the open Arabian Sea (Goericke 2002) and in the California Current Ecosystem (Taniguchi et al. 2014b), which could be due to the high temperature of our system during the summer. It has been suggested that both micro- and picophytoplankton would increase their maximal photosynthesis rate with temperature (Andersson et al. 1994). Furnas & Crosbie (1999) reported maximal *in situ* growth rates of 2.1 d^{-1} for *Synechococcus* and 1.4 d^{-1} for *Prochlorococcus* at the relatively high temperature of 22 to 30°C. These values are close to our estimate of the size-specific maximal growth rate for picoplankton (1.9 ± 0.2 d^{-1}) in the NSCS. The high temperature in the NSCS during the summer compared to other systems in the subtropical oceans could well explain the observed high contribution of picoautotrophs to biomass, as the size of the phytoplankton community would generally decrease with temperature (Chen & Liu 2010). The high temperature might have also resulted in the high grazing rate of microzooplankton on phytoplankton, which will be further discussed in the next section.

The size-dependent phytoplankton grazing mortality on Tchl *a*

We also analyzed the responses of phytoplankton grazing mortality to the ascending Tchl *a* for the 3 phytoplankton size classes in the NSCS (Fig. 4D). There were general increases ($r^2 = 0.57$, $p < 0.05$) of the size-specific grazing mortality rates with Tchl *a* when Tchl *a* was <1 µg l^{-1}. The grazing mortality rates become somewhat saturated for all 3 size classes as the concentration of Tchl *a* continues to increase beyond 1 µg l^{-1} in the coastal zone of the NSCS (Fig. 4D). These results can be explained by the relationship between mass-specific grazing rate (m) and phytoplankton biomass (P) in the following equation:

$$m = \frac{g_0 Z}{\lambda + P} \quad (3)$$

where Z is microzooplankton biomass; g_0 and λ are the maximal grazing rate and half-saturation constant for *Holing II* grazing, respectively. (Li et al. 2011). In the oceanic zone where $P << \lambda$, we will have $m \approx (g_0 Z) / \lambda$. Thus, m will increase with P as Z increases with P. In contrast, when $P >> \lambda$ such as in the productive coastal zone, we should have $m \approx (g_0 Z) / P$, which may be relatively conservative as the Z:P ratio here could decrease with P (Gasol et al. 1997). Saturation grazing was found at Stn P4, as implied by a relatively constant apparent growth rate in the less diluted treatment ($D > 0.7$) for each size class (see Fig. S1). We should point out that the value of λ could be very different between different size classes. Unfortunately, we could not assess λ for various size classes, since we did not have zooplankton biomass data available.

For the entire study region, the maximal grazing rates of different phytoplankton size classes by

microzooplankton can be roughly estimated from our data (Fig. 4D) with 3.1, 2.9, and 2.4 d^{-1} for micro-, nano-, and picophytoplankton, respectively. We cannot group the size-specific grazing rates by different zones since microphytoplankton was mostly not present in the transition and oceanic zones. High maximal grazing rates found in the NSCS may be due to the high temperature of our system, as grazing rates may increase with seawater temperature (Taniguchi et al. 2014b). Interestingly, our results suggest a higher maximal grazing mortality rate for larger phytoplankton in the NSCS (Fig. 4D). This finding is consistent with the observed increase of phytoplankton maximal growth rate with cell size. The coupling between growth and grazing should also explain the relatively small variations in grazing impacts for different size classes shown in the previous sections. Indeed, it was suggested that the temperature-corrected phytoplankton grazing mortality rate would generally increase with phytoplankton cell size based on a global dataset of dilution experiments (Chen & Liu 2010). The positive relationship between phytoplankton grazing mortality rate and cell size might also reflect the spatial change of microzooplankton grazers. The main microzooplankton grazers could be pico- and nano-flagellates in oligotrophic waters dominated by small phytoplankton, whereas heterotrophic and mixotrophic dinoflagellates generally become the major grazers of phytoplankton in productive waters (Calbet 2008).

CONCLUSIONS

Based on data from the size-fractionated chl *a* measurements and size-specific dilution experiments, we found substantial variations in phytoplankton size structure and size-specific phytoplankton growth and grazing mortality rates in the coastal, transition, and oceanic zones of the NSCS. We found high concentrations of microphytoplankton in the inner shelf, in contrast to nanophytoplankton taking over the phytoplankton community in the middle and outer shelves, which could be explained by the enhanced grazing impact on small phytoplankton in the coastal regions. Slow-growing picophytoplankton (mainly *Prochlorococcus* and *Synechococcus*) were the dominant phytoplankton group in the oligotrophic oceanic region of the NSCS. Our results also suggest that the size class of nanophytoplankton in the NSCS might need to be separated into 2 additional subgroups to better represent the variations of *Cryptophytes* and *Prymnesiophytes* with the ascending Tchl *a*.

By examining the functional responses of the size-specific growth rates to the varying ambient nitrate concentrations, we found a much higher maximal growth rate and a larger half-saturation constant for microphytoplankton compared to those for nano- and picophytoplankton. We also assessed the responses of phytoplankton grazing mortality to Tchl *a* for the 3 size classes and found an increase in maximal grazing mortality rate with phytoplankton cell size. These results could provide better parameterizations of size-structured ecosystem models, and thus improve the size-structure modeling of plankton ecosystem and biogeochemical cycles in the NSCS.

Acknowledgements. We are grateful to the captains and staffs of the R/V 'Shiyan III' and 'Zhanjiang Kediao' for their help during the cruises. This work was supported by the National Key Research and Development Program of China (2016YFA0601203-02), the Natural Science Foundation of China (41676108, 41706181) and the Natural Science Foundation of Guangdong Province (2017A030313251).

LITERATURE CITED

Andersson A, Haecky P, Hagström A (1994) Effect of temperature and light on the growth of micro- nano- and pico-plankton: impact of algal succession. Mar Biol 120: 511–520

Brewin RJW, Sathyendranath S, Hirata T, Lavender SJ, Barciela RM, Hardman-Mountford NJ (2010) A three-component model of phytoplankton size class for the Atlantic Ocean. Ecol Modell 221:1472–1483

Cáceres C, Taboada FG, Höfer J, Anadón R (2013) Phytoplankton growth and microzooplankton grazing in the subtropical Northeast Atlantic. PLOS ONE 8:e69159

Cáceres C, Rivera A, González S, Anadón R (2017) Phytoplankton community structure and dynamics in the North Atlantic subtropical gyre. Prog Oceanogr 151: 177–188

Calbet A (2008) The trophic roles of microzooplankton in marine systems. ICES J Mar Sci 65:325–331

Calbet A, Landry MR (2004) Phytoplankton growth, microzooplankton grazing, and carbon cycling in marine systems. Limnol Oceanogr 49:51–57

Calbet A, Saiz E (2005) The ciliate-copepod link in marine ecosystem. Aquat Microb Ecol 38:157–167

Cermeño P, Estévez-Blanco P, Marañón E, Fernández E (2005) Maximum photosynthetic efficiency of size-fractionated phytoplankton assessed by ^{14}C-uptake and fast repetition rate fluorometry. Limnol Oceanogr 50: 1438–1446

Chen BZ, Liu HB (2010) Relationships between phytoplankton growth and cell size in surface oceans: interactive effects of temperature, nutrients, and grazing. Limnol Oceanogr 55:965–972

Chen YLL, Chen HY, Karl DM, Takahashi M (2004) Nitrogen modulates phytoplankton growth in spring in the South China Sea. Cont Shelf Res 24:527–541

Chen BZ, Liu HB, Landry MR, Dai MH, Huang BQ, Sun J (2009) Close coupling between phytoplankton growth

and microzooplankton grazing in the western South China Sea. Limnol Oceanogr 54:1084–1097

Chen MR, Liu HB, Song SQ, Sun J (2015) Size-fractionated mesozooplankton biomass and grazing impact on phytoplankton in northern South China Sea during four seasons. Deep Sea Res II 117:108–118

Chisholm SW (1992) Phytoplankton size. In: Falkowski PG, Woodhead AD (eds) Primary productivity and biogeochemical cycles in the sea. Plenum Press, New York, NY, p 213–237

Ciotti ÁM, Lewis MR, Cullen JJ (2002) Assessment of the relationships between dominant cell size in natural phytoplankton communities and the spectral shape of the absorption coefficient. Limnol Oceanogr 47:404–417

Furnas MJ, Crosbie ND (1999) *In situ* growth dynamics of photosynthetic prokaryotic picoplankters *Synechococcus* and *Prochlorococcus*. In: Charpy L, Larkum AWD (eds) Marine cyanobacteria. Bulletin de l'Institut Océanographique, Spécial 19, Monaco, p 387–417

Gasol JM, del Giorgio PA, Duarte CM (1997) Biomass distribution in marine planktonic communities. Limnol Oceanogr 42:1353–1363

Goericke R (2002) Top-down control of phytoplankton biomass and community structure in the monsoonal Arabian Sea. Limnol Oceanogr 47:1307–1323

Goericke R (2011a) The structure of marine phytoplankton communities: patterns, rules and mechanisms. CCOFI Rep 52:182–197

Goericke R (2011b) The size structure of marine phytoplankton: What are the rules? CCOFI Rep 52:198–204

Hansen HP, Koroleff F (1999) Determination of nutrients. In: Grasshoff K, Kremling K and Ehrhardt M (eds) Methods of seawater analysis, 3rd edn. Wiley-VCH, Weinheim, p 159–228

Huang BQ, Xiang WG, Zeng XB, Chiang KP and others (2011) Phytoplankton growth and microzooplankton grazing in a subtropical coastal upwelling system in the Taiwan Strait. Cont Shelf Res 31:S48–S56

Irwin AJ, Finkel ZV, Schofield OME, Falkowski PG (2006) Scaling-up from nutrient physiology to the size-structure of phytoplankton communities. J Plankton Res 28: 459–471

Kuipers BR, Witte HJ (1999) Grazing impact of microzooplankton on different size classes of algae in the North Sea in early spring and mid-summer. Mar Ecol Prog Ser 180:93–104

Landry MR, Hassett RP (1982) Estimating the grazing impact of marine micro-zooplankton. Mar Biol 67:283–288

Landry MR, Ohman MD, Goericke R, Stukel MR, Tsyrklevich K (2009) Lagrangian studies of phytoplankton growth and grazing relationships in a coastal upwelling ecosystem off southern California. Prog Oceanogr 83: 208–216

Li QP, Franks PJS, Landry MR, Goericke R, Taylor AG (2010) Modeling phytoplankton growth rates and chlorophyll to carbon ratios in California coastal and pelagic ecosystems. J Geophys Res 115:G04003

Li QP, Franks PJS, Landry MR (2011) Microzooplankton grazing dynamics: parameterizing grazing models with dilution experiment data in the Southern California Ecosystem. Mar Ecol Prog Ser 438:59–69

Li QP, Dong Y, Wang YJ (2016) Phytoplankton dynamics driven by vertical nutrient fluxes during the spring intermonsoon period in the northeastern South China Sea. Biogeosciences 13:455–466

Lie AA, Wong CK (2010) Selectivity and grazing impact of microzooplankton on phytoplankton in two subtropical semi-enclosed bays with different chlorophyll concentrations. J Exp Mar Biol Ecol 390:149–159

Litchman E, Klausmeler CA, Schofield OM, Falkowski PG (2007) The role of functional traits and trade-offs in structuring phytoplankton communities: scaling from cellular to ecosystem level. Ecol Lett 10:1170–1181

Liu HB, Chang J, Tseng CM, Wen LS, Liu KK (2007) Seasonal variability of picoplankton in the northern South China Sea at the SEATS station. Deep Sea Res II 54: 14–15

Malone TC (1980) Size-fractionated primary productivity of marine phytoplankton. In: Falkowski PG (ed) Primary productivity in the sea: Brookhaven symposia in biology. Springer, Boston, MA, p 301–309

Marañón E (2015) Cell size as a key determinant of phytoplankton metabolism and community structure. Annu Rev Mar Sci 7:241–264

Marañón E, Cermeño P, Rodríguez J, Zubkov MV, Harris RP (2007) Scaling of phytoplankton photosynthesis and cell size in the ocean. Limnol Oceanogr 52:2190–2198

Moore CM, Mills MM, Arrigo KR, Berman-Frank I and others (2013) Processes and patterns of oceanic nutrient limitation. Nat Geosci 6:701–710

Neuer S, Cowles TJ (1994) Protist herbivory in the Oregon upwelling system. Mar Ecol Prog Ser 113:147–162

Nielsen SL (2006) Size-dependent growth rates in eukaryotic and prokaryotic algae exemplified by green algae and cyanobacteria: comparisons between unicells and colonial growth forms. J Plankton Res 28:489–498

Ning X, Li WKW, Cai Y, Shi J (2005) Comparative analysis of bacterioplankton and phytoplankton in three ecological provinces of the northern South China Sea. Mar Ecol Prog Ser 293:17–28

Olson RJ, Zettler ER, DuRand MD (1993) Phytoplankton analysis using flow cytometry. In: Kemp P, Sherr BF, Sherr EB, Cole JJ (eds) Handbook of methods in aquatic microbial ecology. Lewis Publishers, New York, NY, p 175–186

Pahlow M, Riebesell U, Wolf-Gladrow DA (1997) Impact of cell shape and chain formation on nutrient acquisition by marine diatoms. Limnol Oceanogr 42:1660–1672

Pan XJ, Wong GTF, Ho TY, Shiah FK, Liu HB (2013) Remote sensing of picophytoplankton distribution in the northern South China Sea. Remote Sens Environ 128:162–175

Parsons TR, Maita Y, Lalli CM (1984) A manual of chemical and biological methods for seawater analysis. Pergamum Press, Oxford

Raimbault P, Rodier M, Taupier-Letage I (1988) Size fraction of phytoplankton in the Ligurian Sea and the Algerian Basin (Mediterranean Sea): size distribution versus total concentration. Mar Microb Food Webs 3:1–7

Sherr EB, Sherr BF (2009) Capacity of herbivorous protists to control initiation and development of mass phytoplankton blooms. Aquat Microb Ecol 57:253–262

Sherr EB, Sherr BF, Wheeler PA (2005) Distribution of coccoid cyanobacteria and small eukaryotic phytoplankton in the upwelling ecosystem off the Oregon coast during 2001 and 2002. Deep Sea Res II 52:317–330

Stolte W, McCollin T, Noordeloos AAM, Riegman R (1994) Effect of nitrogen source on the size distribution within marine phytoplankton populations. J Exp Mar Biol Ecol 184:83–97

Strom S (2002) Novel interactions between phytoplankton

and microzooplankton: their influence on the coupling between growth and grazing rates in the sea. Hydrobiologia 480:41–54

Strom SL, Macri EL, Olson MB (2007) Microzooplankton grazing in the coastal Gulf of Alaska: variations in top-down control of phytoplankton. Limnol Oceanogr 52: 1480–1494

Su J (2004) Overview of the South China Sea circulation and its influence on the coastal physical oceanography outside the Pearl River Estuary. Cont Shelf Res 24:1745–1760

Taniguchi AAD, Franks PJS, Landry MR (2012) Estimating size-dependent growth and grazing rates and their associated errors using the dilution method. Limnol Oceanogr Methods 10:868–881

Taniguchi AAD, Franks PJS, Poulin FJ (2014a) Planktonic biomass size spectra: an emergent property of size-dependent physiological rates, food web dynamics, and nutrient regimes. Mar Ecol Prog Ser 514:13–33

Taniguchi AAD, Landry MR, Franks PJS, Selph KE (2014b) Size-specific growth and grazing rates for picophytoplankton in coastal and oceanic regions of the eastern Pacific. Mar Ecol Prog Ser 509:87–101

Thingstad TF (1998) A theoretical approach to structuring mechanisms in the pelagic food web. Hydrobiologia 363: 59–72

Thingstad TF, Øvreås L, Egge JK, Løvdal T, Heldal M (2005) Use of non-limiting substrates to increase size; a generic strategy to simultaneously optimize uptake and minimize predation in pelagic osmotrophs? Ecol Lett 8:675–682

Vaulot D, Courties C, Partensky F (1989) A simple method to preserve oceanic phytoplankton for flow cytometric analyses. Cytometry 10:629–635

Verdy A, Follows M, Flierl G (2009) Optimal phytoplankton cell size in an allometric model. Mar Ecol Prog Ser 379: 1–12

Wang L, Huang BQ, Liu X, Xiao WP (2015) The modification and optimizing of the CHEMTAX running in the South China Sea. Acta Oceanol Sin 34:124–131

Ward BA, Dutkiewicz S, Jahn O, Follows MJ (2012) A size-structured food-web model for the global ocean. Limnol Oceanogr 57:1877–1891

Wu J, Chung S, Wen L, Liu K and others (2003) Dissolved inorganic phosphorus, dissolved iron, and *Trichodesmium* in the oligotrophic South China Sea. Global Biogeochemical Cycles 17:1008–1017

Zhou L, Tan Y, Huang L, Hu Z, Ke Z (2015) Seasonal and size-dependent variations in the phytoplankton growth and microzooplankton grazing in the southern South China Sea under the influence of the East Asian Monsoon. Biogeosciences 12:6809–6822

Editorial responsibility: Steven Lohrenz, New Bedford, Massachusetts, USA

Submitted: July 28, 2017; Accepted: April 27, 2018
Proofs received from author(s): June 22, 2018